Zeeman splitting and dynamics of an isoelectronic bound exciton near the band edge of ZnO

S. L. Chen, W. M. Chen, and I. A. Buyanova*
Department of Physics, Chemistry and Biology, Linköping University, 58183 Linköping. Sweden
(Received 10 October 2012; published 17 December 2012)

Comprehensive time-resolved photoluminescence and magneto-optical measurements are performed on a bound exciton (BX) line peaking at 3.3621 eV (labeled as I^*). Though the energy position of I^* lies within the same energy range as that for donor bound exciton (DX) transitions, its behavior in an applied magnetic field is found to be distinctly different from that observed for DXs bound to either ionized or neutral donors. An exciton bound to an isoelectronic center with a hole-attractive local potential is shown to provide a satisfactory model that can account for all experimental results of the I^* transition.

DOI: 10.1103/PhysRevB.86.235205 PACS number(s): 78.55.Et, 71.35.Ji, 78.20.Ls, 71.55.Gs

I. INTRODUCTION

Being a wide and direct bandgap semiconductor with a very large exciton energy of about 60 meV, ZnO is potentially promising as a light emitter material for the ultraviolet (UV) spectral range and white lighting.[1] It is often considered to be advantageous over its rival material GaN since it is nontoxic and is available in large bulk single crystals of very high quality. It is commonly known that nominally undoped ZnO crystals contain a variety of intrinsic defects and unintentionally incorporated impurities.[2,3] Many of them introduce shallow levels which capture free carriers and free excitons (FXs) at low temperatures to form bound excitons (BXs).[2,4–8] The majority of these BXs in ZnO emit light within a narrow spectral range below the FX transition and give rise to a series of very sharp and intense emission lines that dominate in photoluminescence (PL) at low temperatures. The origin of these emissions has been a subject of intensive research studies over the past decades,[2] since each impurity or defect gives rise to a specific BX emission that in turn can be used for simple and nondestructive determination of its presence in the crystal by optical means. Moreover, analysis of the BX behavior under external perturbations such as a magnetic field may provide additional information not only about the electronic structure of the defect/impurity, but also properties of band states, e.g. ordering of valence band (VB) states.[8–12]

From magneto-optical studies it was established[8,12,13] that most of the BX lines observed in ZnO within the near-band-edge spectral range are due to excitons bound to shallow donors (DXs). Depending on the charge state of the donors, i.e. neutral or positively charged, DXs could be categorized into ionized donor bound exciton (D^+X) and neutral donor bound exciton (D^0X). The former usually has a higher transition energy than the latter. When forming D^+X and D^0X, the participating holes may belong to one of the valence subbands.[2,14,15] This is because the electron and hole which form the exciton are only weakly bound to the donor and, therefore, retain their band characters.[9] Energies of the D^0X transitions that involve B-VB holes (D^0X^B) are higher by ~4.5 meV than their D^0X^A counterparts, as determined by the splitting between A- and B-VB subbands. (For D^+Xs, only transitions that involve A-VB holes were detected so far in photoluminescence). The charge state of DX (D^0X or D^+X) could be distinguished from magneto-PL measurements performed, e.g. with a magnetic field B applied perpendicular to the c axis of ZnO. Indeed, in this measurement geometry D^+X shows the appearance of an additional component that is located at the low energy side of the main line (i.e. the one observed at $B = 0$) and gains its intensity with increasing B. This is in sharp contrast with D^0X, which exhibits symmetrically split Zeeman components. From magneto-PL, the origin of the hole involved in the D^0X complex could also be credibly determined,[8,12,15] due to different values and signs of g-factors for the A- and B-VB holes which leads to distinct Zeeman patterns of the D^0X^A and D^0X^B transitions.

In addition to the aforementioned DX-related transitions, a new class of BX lines has most recently been reported in bulk ZnO single crystals[13] though their origin remains unknown. Despite that the energy positions of these lines lie within the same energy range as that for the DX transitions, their behavior in an applied magnetic field is distinctly different from either D^+X or D^0X. Furthermore, the new lines can not be related to excitons bound to shallow acceptors (AXs), since the latter exhibits similar Zeeman pattern as DXs.[6,8] The purpose of this paper is to gain in-depth understanding of the origin of these transitions with the focus on the most prominent line with the energy position of 3.3621 eV. By employing time-resolved PL spectroscopy, we will show that this emission most likely originates from the exciton ground state(s) and does not stem from an excited state of a DX. The electronic structure of the involved exciton will be evaluated based on comprehensive magneto-PL studies complemented by temperature-dependent magneto-absorption measurements.

II. SAMPLES AND METHODS

The samples studied in this paper were commercially available c plane undoped bulk ZnO single crystals from Cermet Inc. and Tokyo Denpa Co. Magneto-optical measurements were performed within the temperature range of 2–15 K in a split-coil superconducting magnet providing magnetic fields up to 11 T. A wavelength tunable, pulsed Ti:sapphire laser with a repetition rate of 76 MHz, a pulse duration of ~150 fs, and a pulse spectral width of 1 nm was employed to carry out magnetotransmission and time-resolved PL measurements. Transient PL was detected by a streak camera combined with a 0.5-m single grating monochromator. A continuous-wave (cw) solid-state laser emitting at 266 nm was used as an excitation source in cw-PL measurements. The cw-PL signal was detected by a photomultiplier tube (PMT) assembled with a 0.8-m double-grating monochromator. The magneto-PL

studies were performed in both Faraday configuration with $\mathbf{B} \parallel \mathbf{c}$ and $\mathbf{k} \parallel \mathbf{c}$ and Voigt configuration with $\mathbf{B} \perp \mathbf{c}$ and $\mathbf{k} \parallel \mathbf{c}$. Here, $\mathbf{k}$ denotes the wave vector of the emitted light, $\mathbf{c}$ and $\mathbf{B}$ are the directions of the crystallographic c axis of ZnO and an applied magnetic field, respectively. In addition, the angle θ between $\mathbf{B}$ and $\mathbf{c}$ was varied in magnetic fields of 4 and 10 T by rotating the sample in the $(11\bar{2}0)$ plane. Circular polarization of emission in the Faraday geometry was analyzed by using a quarter-wave plate and a linear polarizer. The latter was also used to analyze linear polarization of the emission measured in the Voigt configuration. Magnetotransmission measurements were performed at 0 and 4 T in the Voigt configuration.

III. EXCITON DYNAMICS

Figure 1(a) shows a typical PL spectrum measured at 2 K from the Cermet ZnO. As commonly observed in good-quality single-crystalline materials, low-temperature PL is governed by excitonic transitions within the near-band-edge spectral range. The dominant transitions, labeled as I_4, I_6, I_7, and I_8 following notations from Ref. 14, arise from D^0X^A. Spectrally broader peaks that lie about 4.1–4.5 meV above the I_6 and I_4 are associated with their excited states I_6^B and I_4^B, i.e. represent D^0X^B.[14] Transitions related to other excited states of D^0X from, for example, vibrational-rotational and electronic excited states of D^0X^A are visible in excitation spectra of D^0X[6,14] but are usually very weak in emission at 2 K and, therefore, do not contribute to the PL spectra. The I_0 PL line stems from D^+X^A which are typically observed just below the FX_A transitions within the 3.371–3.373 eV spectral range.

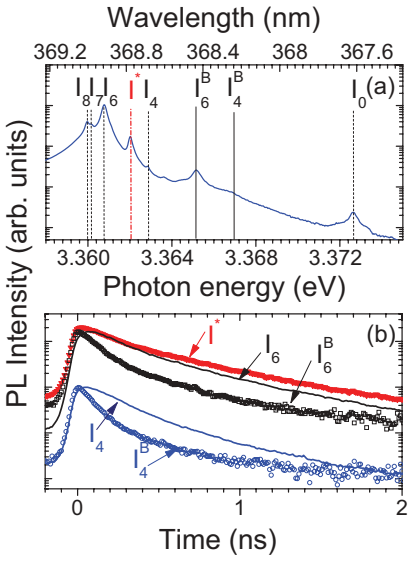

FIG. 1. (Color online) (a) Photoluminescence spectrum measured at 2 K. The ground state bound exciton transitions are marked by the dashed lines, among which I_4, I_6, I_7, and I_8 are D^0X^A states. On the high-energy side lie the excited states of the I_4 and I_6 lines, labeled by I_4^B and I_6^B (marked by the solid lines), respectively. (b) PL decays measured at 2 K from two pairs of D^0X^A and D^0X^B transitions, i.e. I_6 (the solid line)/I_6^B (open squares) and I_4 (the solid line)/I_4^B (open circles). They are offset vertically for clarity. The PL decay of the I^* line is shown by the top curve (the filled triangles). For easy comparison, all curves are normalized to the same peak intensity.

In addition to these D^0X and D^+X transitions, all investigated samples exhibit a rather strong emission line I^* with the energy position of 3.3621 eV which is the focus of this paper. We note that the spectral position of this line is very close to that reported for the I_{4a} transition,[14] though it is currently not clear whether I_{4a} and I^* have the same origin.

As will be shown below, magneto-optical properties of I^* differ considerably from either D^0X or D^+X transitions. On the other hand, they are consistent with a Zeeman pattern observed for the group of lines of unknown origin (lines 5, 7, and 10) that were reported by Ding *et al.*[13] It is therefore most likely that I^* is identical to line 5 in Ref. 13. Based on its energy position, it was suggested[14] that this transition could originate from an excited vibrational-rotational state of I_6. This suggestion, however, seems to be somewhat questionable judging from the high intensity of I^* at 2 K which is usually characteristic for transitions that involve a ground state of an exciton. In principle, emissions from excited and ground states of an exciton could be distinguished by analyzing exciton dynamics.[15,16] Indeed, fast energy relaxation from excited to the ground exciton state shortens lifetime of the former, which is reflected by a fast initial decay of the corresponding emission. To clarify whether I^* stems from an excited or the ground exciton state, we have performed transient PL measurements. The corresponding results are presented in Fig. 1(b), which shows transients of I^* (solid symbols) and several D^0X^A (solid lines) and D^0X^B (open symbols) transitions. We can see that transient dynamics of I^* are very similar to that of the I_6 and I_4 lines related to the ground state of the corresponding bound excitons. It exhibits a relatively fast rising, within 100–150 ps, which likely reflects trapping to the BX state. The subsequent decay is bi-exponential and contains two components with the characteristic times of 0.25 and 0.7 ns. These components most likely represent lifetimes of the I^* excitons generated in different spatial regions of the sample, though they could also be related to degeneracy of the exciton ground state, as will be discussed below. Most importantly, the measured decay times are slightly longer than that for the I_6 and I_4 lines related to the ground D^0X^A states. This is in sharp contrast with the decays of the I_6^B and I_4^B transitions that are dominated by a fast initial decay with a characteristic time of around 120 ps, which reflects exciton relaxation from the excited D^0X^B to the ground D^0X^A state assisted by emission of acoustic phonons.[15,16] Therefore, both the high intensity of the I^* line and its slow transient behavior are more consistent with the assumption that this transition stems from the ground state of the bound exciton.

We also note that lifetimes of shallow D^0X^A excitons have been shown[17] to depend on exciton localization energies and scale as predicted by the model of Rashba and Gurgenishvili.[18] However, the lifetime of the I^* line does not follow this trend which clearly indicates that it cannot arise from the same type of defects as those responsible for the I_4–I_9 lines.

IV. MAGNETO-OPTICAL PROPERTIES

A. Magnetophotoluminescence

Let us now discuss magneto-optical properties of the I^* transition. Figure 2 shows magneto-PL spectra measured

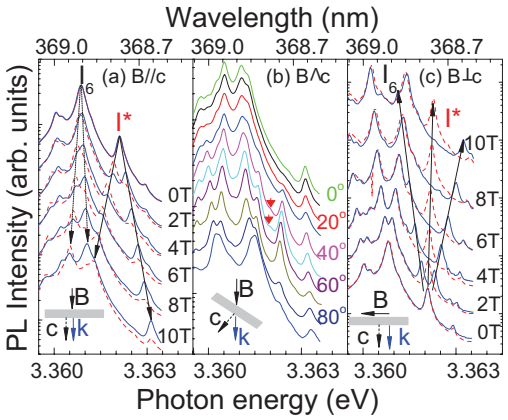

FIG. 2. (Color online) (a) Magneto-PL spectra of the I^* line measured in the Faraday configuration ($\mathbf{B} \parallel \mathbf{c}$), where σ^+ and σ^- polarization are shown by the solid and dashed lines, respectively. (b) Angular dependence of the I^* line at 10 T when the magnetic field is rotated between $\mathbf{B} \parallel \mathbf{c}$ and $\mathbf{B} \perp \mathbf{c}$. (c) Magneto-PL spectra of the I^* line measured in the Voigt configuration ($\mathbf{B} \perp \mathbf{c}$), by monitoring the polarization $\mathbf{E} \perp \mathbf{B}$ (the solid curves) and $\mathbf{E} \parallel \mathbf{B}$ (the dashed curves). The spectra for different field strengths or different rotating angles are vertically shifted for clarity.

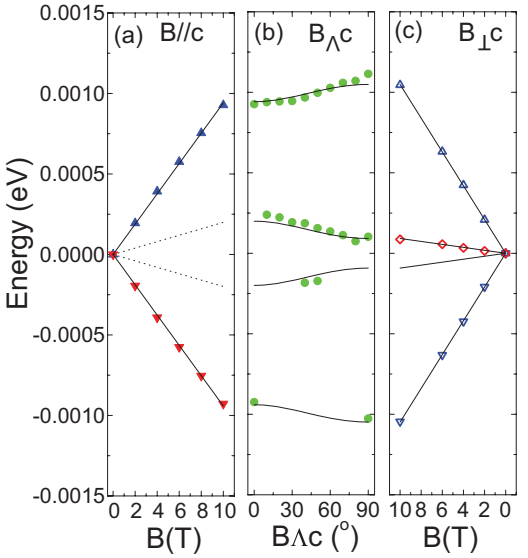

FIG. 3. (Color online) Zeeman splitting of the I^* line as a function of magnetic field in the (a) Faraday and (c) Voigt configurations. (b) Angular dependence of the I^* line at 10 T when the magnetic field is rotated by an angle from the $\mathbf{c}$ axis towards $\mathbf{B} \perp \mathbf{c}$. All energy positions are plotted with respect to the center of gravity of the Zeeman split components. The symbols represent experimental results, while lines are fitting curves by the effective spin Hamiltonian Eq. (1) with $g_e = 1.97$, $g_h^{\parallel} = 1.28$, and $g_h^{\perp} = 1.65$. The solid and dashed lines denote allowed and forbidden transitions, respectively.

within the spectral range corresponding to the I^* and I_6 lines. In the Faraday geometry ($\mathbf{B} \parallel \mathbf{c}$, $\mathbf{k} \parallel \mathbf{c}$), I^* exhibits linear splitting into two components that are circularly polarized, see Fig. 2(a). The upper (lower) component is predominantly active in the σ^+ (σ^-) polarization, shown by the solid (the dotted) lines in Fig. 2(a). The same lines are also detected when $\mathbf{B} \parallel \mathbf{c}$ but $\mathbf{k} \perp \mathbf{c}$ (not shown in the figure). The magnitude of the splitting between the two Zeeman components could be described by an effective exciton g-factor of $g_{\text{exc}}^{\parallel} = 3.25$. When the magnetic field direction deviates from the c axis [Fig. 2(b)], the upper component slightly shifts towards higher energies. The emission that stems from the σ^- state strongly overlaps with Zeeman components of the neighboring I_6 line and, therefore, is not resolved in the angular-dependent spectra measured at B = 10T. Angular dependence of this component can be followed, however, at lower magnetic fields. Measurements performed at B = 4T show that this component is slightly anisotropic to the same extent as the higher energy component and shifts to lower energies with increasing angle θ (not shown in Fig. 2). In addition, two new Zeeman lines located in the proximity to the zero field position of I^* appear when the direction of the magnetic field does not coincide with the c axis. These new components have noticeably different intensities: Whereas the higher energy line is intense for all $\theta \neq 0°$, the lower energy line is very weak and is seen only at certain angles of $\theta = 40 - 50°$, indicated by the red arrows in Fig. 2(b). In the Voigt configuration ($\mathbf{B} \perp \mathbf{c}$ and $\mathbf{k} \parallel \mathbf{c}$), all dominant Zeeman components become linearly polarized with the outer pair emitting in ($\mathbf{E} \perp \mathbf{B}, \mathbf{E} \perp \mathbf{c}$) and the inner component in $\mathbf{E} \parallel \mathbf{B}$ polarizations [see Fig. 2(c)]. Here, $\mathbf{E}$ denotes the electric field vector of the emitted light. The inner component is also detected in $\mathbf{E} \parallel \mathbf{c}$ polarization when the measurement geometry is changed to $\mathbf{k} \parallel \mathbf{B}, \mathbf{B} \perp \mathbf{c}$ (not shown in Fig. 2). The energy positions of all Zeeman components of I^* are plotted as a fan diagram in Fig. 3. The data are plotted with respect to the energy corresponding to the center of gravity of the Zeeman split components, to compensate for an overall shift of I^* due to a diamagnetic shift ($<10^{-6}$eV/T^2). The splitting between the outer components when $\mathbf{B} \perp \mathbf{c}$ corresponds to an effective exciton g-value close to 3.62. We note that the deduced excitonic g-factors are significantly larger than reported values for D^0X and D^+X transitions that involve effective mass holes from A-[8,13] or B-VB[15,19] subbands, as well as for the known deeply bound excitons (the so-called Y lines[17]).

B. Thermalization between Zeeman components

Appearance of four Zeeman components could, in principle, be accounted for by the following two models. In the first model, the I^* line originates from an optical transition between two doublets, i.e. from a doublet excited state (e.g. exciton) to a doublet ground state (i.e. without exciton), as shown schematically by the diagram I in Fig. 4(a). This is similar to the case of the D^0X or A^0X transitions involving a given VB subband hole, where both excited [labeled as E in Fig. 4(a)] and ground [labeled as G in Fig. 4(a)] states split into two Zeeman sublevels and the size of the splitting is determined by the g-values of spin unpaired particles. In the second model, the observed Zeeman pattern may be caused by quadruple splitting of the excited state in an applied magnetic field, whereas the ground state is a singlet, see the energy diagram II in Fig. 4(a). This situation occurs for free excitons, ionized donor (or acceptor) bound excitons, excitons bound to isoelectronic centers as well as for donor-acceptor pair (DAP) transitions. The aforementioned two models can be distinguished by analyzing thermalization behavior within the Zeeman sublevels

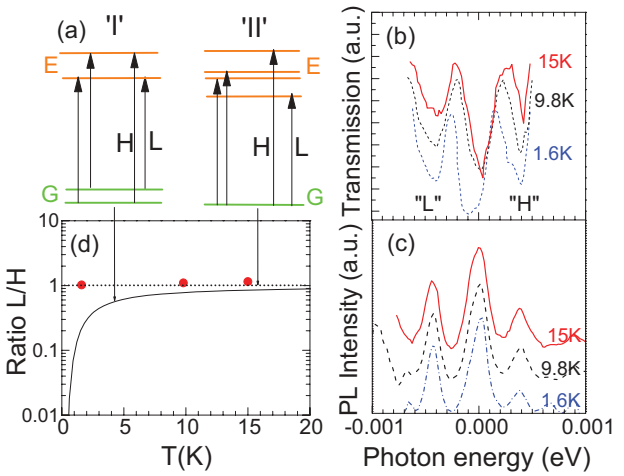

FIG. 4. (Color online) (a) "I" shows the transition scheme of a neutral donor bound exciton (D^0X) where both ground (G) and excited (E) state of the transition are doubly degenerate that split in a magnetic field. "II" represents the transition scheme related to a bound exciton at an isoelectronic center which has a nondegenerate ground state and four sublevels for the excited state (i.e. BX state). The optical transitions with the highest and lowest energies are labeled as H and L, respectively. (b) Magnetotransmission and (c) magnetophotoluminescence spectra measured at different temperatures under a magnetic field of 4 T in the Voigt configuration. For comparison, all spectra have been shifted in energy to counteract the temperature-induced red shift. (d) The absorption ratio between the L and H component as a function of temperature, expected from the thermalization in the ground state if it is a doublet (the solid line) in scenario I and a singlet (the dashed line) in scenario II. The filled circles represent the experimental data.

measured in absorption and emission, since the thermalization of the absorption components is solely determined by the energy splitting in the ground state, whereas that of the emission components is only governed by the Zeeman-split excited state. As an example, the expected temperature dependence of the intensity ratio between the absorption components at the lowest (L) and highest (H) energy is depicted in Fig. 4(d) for both models, i.e. the solid line for model I and dashed line for model II. The simulations were done under the assumptions that (a) both components have the same oscillator strength, and (b) the populations among the sublevels of the ground state (G) follow the Boltzmann distribution at thermal equilibrium. The splitting between the sublevels was assumed to be equal to half of the energy spacing between the H and L components, i.e. 0.42 meV at B = 4T. As expected, the ratio is strongly temperature dependent in model I as the lower-lying sublevel of the doublet ground state is increasingly favored with decreasing temperature. In sharp contrast, no temperature dependence is expected in model II, where no thermal redistribution applies to the singlet ground state.

To identify which of the two models is valid for the studied I^* line, we have carried out a temperature-dependent magnetotransmission study at 4 T in the Voigt geometry. The results are shown in Fig. 4(b). To facilitate a direct comparison between the spectra measured at different temperatures, they were shifted in energy to compensate for the temperature-induced change of the ZnO bandgap energy. Three absorption dips [Fig. 4(b)] are clearly resolved in the transmission spectra. Their relative strengths remain nearly constant with rising temperature. The intensity ratio between the L and H lines is also plotted in Fig. 4(d), showing excellent agreement with the simulated temperature dependence from model II. These experimental results provide strong evidence that the ground state of the I^* transition is a singlet. Therefore, the observed Zeeman splitting should occur in the excited state. This is further supported by the results from the temperature-dependent PL measurements [Fig. 4(c)], carried out under the same experimental conditions as the magnetotransmission (i.e. at 4 T in Voigt geometry). A thermal redistribution between the spin-split sublevels in the excited state is observed with increasing temperature, evident from the increasing intensity of the highest-energy PL component with respect to the lowest-energy one.

From these magnetotransmission and magneto-PL studies, we can conclude that the ground state of the center responsible for the I^* line should have a total effective spin S = 0, i.e. with no bound electrons or holes with unpaired spins. In the excited state, on the other hand, the center should contain two bound particles of effective spin 1/2 giving rise to a total of four electronic and spin sublevels as observed in our experiments. The involved particles can be described by a bound electron and hole pair forming a bound exciton. Possible candidates of defect centers that can possess such electronic structure are an isoelectronic center, an ionized donor, an ionized acceptor, and distant DAP. The possibility of an ionized acceptor can be ruled out here based on the absence of the emissions from neutral acceptor bound excitons in the studied ZnO crystals, which are expected to be much stronger than ionized acceptor bound exciton emissions. For an ionized donor bound exciton, the bound hole should be effective-masslike with a g-factor similar to that of a VB hole. The observed large deviation of the hole g-value of the studied center from that of the VB hole, to be presented below, also excludes an ionized donor from being responsible. This leaves an isoelectronic center as the most likely candidate. (Generally speaking, the last alternative also includes DAP transitions, as electronic structure of a DA pair is equivalent to that of an isoelectronic center with a negligible exchange interaction between the trapped electron and hole).

C. Group theory consideration

Let us now discuss in more detail the electronic structure of the center responsible for the I^* line, starting from group theory considerations. First of all, we note that all Zeeman components of I^* are strongly polarized, as determined by the direction of the applied magnetic field. This means that the monitored optical transitions obey strict selection rules, which is only possible if the involved center has high symmetry. The highest symmetry group of a substitutional impurity in wurtzite matrix is C_{3v} where the bound electron and hole will likely have Γ_4 symmetry (though weakly bound states at substitutional impurities such as DX may be adequately described within the C_{6v} point group of the crystal[9]). The possible symmetries of exciton states can then be derived as the Kronecker product of the electron and hole representations, i.e. $\Gamma_4 \otimes \Gamma_4 = \Gamma_1 \oplus \Gamma_2 \oplus \Gamma_3$. The ground state of the I^*

transition is a singlet state of Γ_1 symmetry without the exciton. According to selection rules, the nondegenerate Γ_1 exciton and the doubly degenerate Γ_3 exciton are dipole allowed in $\mathbf{E}\parallel\mathbf{c}$ and $\mathbf{E}\perp\mathbf{c}$ polarization, respectively, whereas the nondegenerate Γ_2 exciton is dipole forbidden. (Though the Γ_1 exciton is dipole allowed, it is spin forbidden as will be discussed below.) The Γ_3 (Γ_1) states correspond to a total (i.e. including spin and orbital contributions) angular momentum projection of ± 1 (0). Splitting between the states in zero field is determined by combined effects of electron-hole exchange and spin-spin exchange interactions. It is very small for I^*, i.e. below 0.01 meV, and could not be spectrally resolved (due to a relatively broad line width of the I^* line; see Figs. 2 and 3).

A qualitative understanding of the magneto-optical properties of the I^* line can also be obtained by applying group theory analysis. When applying field along the c axis ($\mathbf{B}\parallel\mathbf{c}$), the point symmetry is reduced to C_3. As a result, irreducible representations change as $\Gamma_3 \rightarrow \Gamma_3 + \Gamma_2$, which are allowed for circular-polarized emission with $\mathbf{E}\perp\mathbf{c}$ as is observed for the outer components of I^* in the Faraday geometry. The Γ_2 state is reduced to Γ_1, whereas the Γ_1 state retains its symmetry. Though both of these states are now dipole allowed for linearly polarized light with $\mathbf{E}\parallel\mathbf{B}$, they remain spin forbidden and do not contribute to the PL spectra, as will be discussed below. When the magnetic field is directed perpendicular to the c axis ($\mathbf{B}\perp\mathbf{c}$), the C_{3v} symmetry is lowered to C_s. The original Γ_1 and Γ_2 remain their symmetries, but both are now dipole allowed. The Γ_3 state, on the other hand, evolves into Γ_1 and Γ_2. The transitions from Γ_1 states emit photons with $\mathbf{E}\parallel\mathbf{B}$,$\mathbf{E}\perp\mathbf{c}$ and also $\mathbf{E}\perp\mathbf{B}$, $\mathbf{E}\parallel\mathbf{c}$ polarizations because the unitary and reflection operations of the light polarization about the symmetry plane defined by the field and c axis results in the Γ_1 representation. As for Γ_2 states, the same symmetry operations allows the emission of photons with $\mathbf{E}\perp\mathbf{B}$, $\mathbf{E}\perp\mathbf{c}$. These predictions again agree well with our experimental results measured when $\mathbf{B}\perp\mathbf{c}$, if we assume that the outer (inner) components stem from the Γ_2 (Γ_1) states.

D. Effective spin Hamiltonian analysis

To obtain quantitative information on the magneto-optical properties of the I^* line, we resort to an analysis of the experimentally observed Zeeman pattern by the following effective spin Hamiltonian for BX at an isoelectronic center:

$$H = \mu_B \mathbf{B}\cdot\mathbf{g}_e\cdot\mathbf{S}_e + \mu_B\mathbf{B}\cdot\mathbf{g}_h\cdot\mathbf{S}_h. \quad (1)$$

(We note that, even though this spin Hamiltonian is constructed for the BX states, the analysis presented in this section is also valid for donor-acceptor pair transitions as exchange interaction is very weak for I^*.) Here, μ_B is the Bohr magneton; $\mathbf{S}_e$ and $\mathbf{S}_h$ are the effective spins of the electron and hole forming the BX state, respectively, with $\mathbf{S}_e = 1/2$ and $\mathbf{S}_h = 1/2$; $\mathbf{g}_e$ ($\mathbf{g}_h$) is the electron (hole) g-tensor. From a best fit of the spin Hamiltonian to the experimental data, shown as solid lines in Fig. 3, the electron g-tensor is found to be isotropic and is thus reduced to a scalar $g_e = 1.97$. The hole g-tensor, on the other hand, is concluded to be axial along the c axis with the principle hole g-values of $g_h^{\parallel} = 1.28$, $g_h^{\perp} = 1.65$.

The A-VB hole states are derived from the p orbital state, with a mixture of $|\pm 1\rangle$ and $|0\rangle$ character such that the hole g-factor is strongly anisotropic but $g_h^{\perp} \neq 0$. Here, $|m_l\rangle$ denotes the orbital state with a magnetic quantum number m_l of the orbital angular momentum ($l = 1$), which defines the polarization of electric-dipole allowed optical transitions. The observed reduction in the degree of anisotropy of the hole g-factor as well as significant changes of its values for the I^* BX suggests that the involved hole is no longer weakly bound and, therefore, does not originate from the top valence band. This can be modeled, for example, by an increased contribution from the $|0\rangle$ state caused by the spin-orbit interaction and local crystal field of the I^* center, as compared with the A-VB state. The eigenvalues and eigenstates of the four BX sublevels are listed in Table I. When $\mathbf{B}\parallel\mathbf{c}$, the optical transitions from the outer two sublevels of the BX to the ground state are both electric-dipole and spin allowed, emitting $\sigma^{\pm}$ light. The inner two sublevels, on the other hand, are spin forbidden

TABLE I. Eigenenergies and eigenstates of the I^* BX when $\mathbf{B} = \mathbf{B_z}\parallel\mathbf{c}$ and $\mathbf{B} = \mathbf{B_x}\perp\mathbf{c}$. The basis set of wave functions $|m_j\rangle_h|m_s\rangle_e$ is a product of the hole and electron state, where m_j and m_s denote the projections of the effective hole and electron spin angular momentum along the c axis, respectively. Here, $|+\frac{1}{2}\rangle_e = |\uparrow\rangle$ and $|-\frac{1}{2}\rangle_e = |\downarrow\rangle$; $|+\frac{1}{2}\rangle_h = -\gamma|+1,\Downarrow\rangle - \delta|0,\Uparrow\rangle$ and $|-\frac{1}{2}\rangle_h = \gamma|-1,\Uparrow\rangle + \delta|0,\Downarrow\rangle$, where $|m_l,\Uparrow\rangle$ ($|m_l,\Downarrow\rangle$) denotes the hole state constructed from the orbital state $|m_l\rangle$ and spin-up (spin-down) spin state. The parameters γ and δ describe the contributions from the $|m_l = \pm 1\rangle$ and $|m_l = 0\rangle$ state of the hole, with $\gamma^2 + \delta^2 = 1$ and $\gamma^2 \gg \delta^2$; $|X\rangle_{\rm ex} = \frac{1}{\sqrt{2}}(|+\frac{1}{2}\rangle_h|+\frac{1}{2}\rangle_e - |-\frac{1}{2}\rangle_h|-\frac{1}{2}\rangle_e)$; $|Y\rangle_{\rm ex} = -\frac{i}{\sqrt{2}}(|+\frac{1}{2}\rangle_h|+\frac{1}{2}\rangle_e + |-\frac{1}{2}\rangle_h|-\frac{1}{2}\rangle_e)$; $|t\rangle_{\rm ex} = -\frac{1}{\sqrt{2}}(|+\frac{1}{2}\rangle_h|-\frac{1}{2}\rangle_e + |-\frac{1}{2}\rangle_h|+\frac{1}{2}\rangle_e)$; $|z\rangle_{\rm ex} = -\frac{i}{\sqrt{2}}(|+\frac{1}{2}\rangle_h|-\frac{1}{2}\rangle_e - |-\frac{1}{2}\rangle_h|+\frac{1}{2}\rangle_e)$.

Direction of **B**	Eigenenergy	Eigenstate	Polarization
$\mathbf{B_z}\parallel\mathbf{c}$	$+\frac{1}{2}\mu_B B(g_e + g_h^{\parallel})$	$\lvert+\frac{1}{2}\rangle_h\lvert+\frac{1}{2}\rangle_e = -\gamma\lvert+1,\Downarrow\rangle\lvert\uparrow\rangle - \delta\lvert 0,\Uparrow\rangle\lvert\uparrow\rangle$	σ^+
	$+\frac{1}{2}\mu_B B(g_e - g_h^{\parallel})$	$\lvert-\frac{1}{2}\rangle_h\lvert+\frac{1}{2}\rangle_e = \gamma\lvert-1,\Uparrow\rangle\lvert\uparrow\rangle + \delta\lvert 0,\Downarrow\rangle\lvert\uparrow\rangle$	π (negligibly weak)
	$-\frac{1}{2}\mu_B B(g_e - g_h^{\parallel})$	$\lvert+\frac{1}{2}\rangle_h\lvert-\frac{1}{2}\rangle_e = -\gamma\lvert+1,\Downarrow\rangle\lvert\downarrow\rangle - \delta\lvert 0,\Uparrow\rangle\lvert\downarrow\rangle$	π (negligibly weak)
	$-\frac{1}{2}\mu_B B(g_e + g_h^{\parallel})$	$\lvert-\frac{1}{2}\rangle_h\lvert-\frac{1}{2}\rangle_e = \gamma\lvert-1,\Uparrow\rangle\lvert\downarrow\rangle + \delta\lvert 0,\Downarrow\rangle\lvert\downarrow\rangle$	σ^-
$\mathbf{B_x}\perp\mathbf{c}$	$+\frac{1}{2}\mu_B B(g_e + g_h^{\perp})$	$\frac{1}{2}(\lvert-\frac{1}{2}\rangle_h\lvert-\frac{1}{2}\rangle_e + \lvert+\frac{1}{2}\rangle_h\lvert-\frac{1}{2}\rangle_e + \lvert-\frac{1}{2}\rangle_h\lvert+\frac{1}{2}\rangle_e + \lvert+\frac{1}{2}\rangle_h\lvert+\frac{1}{2}\rangle_e) = \frac{i}{\sqrt{2}}(\lvert Y\rangle_{\rm ex} + i\lvert t\rangle_{\rm ex})$	$\mathbf{E}\perp\mathbf{B}$,$\mathbf{E}\perp\mathbf{c}$
	$+\frac{1}{2}\mu_B B(g_e - g_h^{\perp})$	$\frac{1}{2}(\lvert-\frac{1}{2}\rangle_h\lvert-\frac{1}{2}\rangle_e - \lvert+\frac{1}{2}\rangle_h\lvert-\frac{1}{2}\rangle_e + \lvert-\frac{1}{2}\rangle_h\lvert+\frac{1}{2}\rangle_e - \lvert+\frac{1}{2}\rangle_h\lvert+\frac{1}{2}\rangle_e) = -\frac{1}{\sqrt{2}}(\lvert X\rangle_{\rm ex} + i\lvert z\rangle_{\rm ex})$	$\mathbf{E}\parallel\mathbf{B}$ and $\mathbf{E}\parallel\mathbf{c}$
	$-\frac{1}{2}\mu_B B(g_e - g_h^{\perp})$	$\frac{1}{2}(\lvert-\frac{1}{2}\rangle_h\lvert-\frac{1}{2}\rangle_e + \lvert+\frac{1}{2}\rangle_h\lvert-\frac{1}{2}\rangle_e - \lvert-\frac{1}{2}\rangle_h\lvert+\frac{1}{2}\rangle_e - \lvert+\frac{1}{2}\rangle_h\lvert+\frac{1}{2}\rangle_e) = -\frac{1}{\sqrt{2}}(\lvert X\rangle_{\rm ex} - i\lvert z\rangle_{\rm ex})$	$\mathbf{E}\parallel\mathbf{B}$ and $\mathbf{E}\parallel\mathbf{c}$
	$-\frac{1}{2}\mu_B B(g_e + g_h^{\perp})$	$\frac{1}{2}(-\lvert-\frac{1}{2}\rangle_h\lvert-\frac{1}{2}\rangle_e + \lvert+\frac{1}{2}\rangle_h\lvert-\frac{1}{2}\rangle_e + \lvert-\frac{1}{2}\rangle_h\lvert+\frac{1}{2}\rangle_e - \lvert+\frac{1}{2}\rangle_h\lvert+\frac{1}{2}\rangle_e) = -\frac{i}{\sqrt{2}}(\lvert Y\rangle_{\rm ex} - i\lvert t\rangle_{\rm ex})$	$\mathbf{E}\perp\mathbf{B}$,$\mathbf{E}\perp\mathbf{c}$

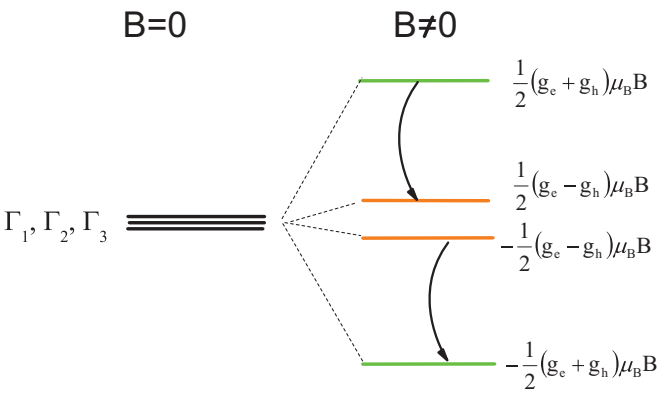

FIG. 5. (Color online) Energy level scheme of the I^* BX with and without magnetic field. The fast hole spin relaxation process is denoted by the arrows, which explains the PL intensity difference between the two middle lines. The hole g-factor is defined as $g_h = \sqrt{(g_h^{\parallel}\cos(\theta))^2 + (g_h^{\perp}\sin(\theta))^2}$.

except for a contribution due to mixing with the $|0\rangle$ state. For the A-VB states in ZnO, this mixing has experimentally been determined to be less than 0.1%.[20] Though it should be larger for a hole localized at the I^* center judging from the substantially larger values of $g_h^{\perp}$ as compared with that for the A-VB hole ($g_h^{\perp} = 0.22$) and also the observed changes in the value and sign of $g_h^{\parallel}$, the mixing is still too weak to be observed in our experiments (meaning $\gamma > \delta$). When the magnetic field is directed off the c axis, all four components become allowed in optical transitions due to the mixing of wave functions among them. This is consistent with our experimental results. When $\mathbf{B}\perp\mathbf{c}$, the outer PL components are linearly polarized with $\mathbf{E}\perp\mathbf{B}$, $\mathbf{E}\perp\mathbf{c}$, whereas the inner component can be detected either in $\mathbf{E}\parallel\mathbf{B}$, $\mathbf{E}\perp\mathbf{c}$ or $\mathbf{E}\perp\mathbf{B}$, $\mathbf{E}\parallel\mathbf{c}$ polarizations, see Table I. The deduced polarizations are in excellent agreement with those experimentally observed for the I^* Zeeman components (Figs. 2 and 3). The reason for the observed large difference in the PL intensity between the two inner sublevels (Figs. 2 and 3) can be attributed to faster spin relaxation of the hole as compared with the electron, such that the higher-energy inner sublevel accumulates in population, whereas the lower-energy one is rapidly depleted. The related spin relaxation processes are schematically shown in Fig. 5.

V. ELECTRONIC STRUCTURE AND POSSIBLE ORIGIN

It is generally known for isoelectronic BXs and D^+Xs in semiconductors that zero-field splitting is determined by combined effects of electron-hole interactions and local crystal field. The zero-field splitting between the Γ_1 and Γ_2 states has previously been shown[8,9,21] to be small in ZnO and is not resolved for the reported D^+X transitions. On the other hand, the zero-field splitting between the Γ_3 and Γ_1/Γ_2 states is typically of the order of 1 meV for FX and D^+X.[8,19–23] This value is considerably larger than that for I^*, which implies a substantially weaker overlap between the electron and hole wave functions. Several models can, in principle, account for this behavior. First of all, it could occur for DAP lines that correspond to relatively close discrete pairs. Assuming an acceptor ionization energy of ~160 meV (which is a reasonable value for ZnO), I^* should correspond to the DAP pair with the partners separated by around 13.5 Å. Such model can then also justify the experimentally observed appearance of several lines with g-values very similar to the I^* transition (i.e. lines 7 and 10 from Ref. 13 or the line at 3.3640 detected in our samples, which is likely equivalent to line 7). The DAP model, however, cannot explain several experimental observations such as the absence of other discrete DAP lines which should be observable within the same energy range for both type I and type II pair transitions, i.e. when the donor and acceptor occupy either the same or different sublattice sites, respectively. Furthermore, though the I^* line was detected in all investigated Cermet and Denpa samples, the other lines with similar magneto-optical properties (e.g. the 3.3640 eV transition), can only be seen in one of them. Additionally, we cannot detect any DAP emission related to distant pairs in our samples. All these inconsistencies make the DAP model unlikely. The second and much more probable alternative is that the I^* center is an isoelectronic complex defect formed from two or more partners, which are close enough to be favorably formed but distant enough to ensure a weak wave function overlap. The involved defect should consist of grown-in intrinsic defects or common contaminants, or a complex of both, judging from the observation of I^* in undoped bulk ZnO grown by different methods.

In a semiconductor, BXs bound to isoelectronic centers can chiefly be categorized by the so-called electron-attractive or hole-attractive isoelectronic centers in terms of their local potential.[24,25] In formation of a BX at an isoelectronic center with an electron-attractive local potential, an electron is bound first followed by binding of a hole in a Coulomb-like potential from the primary bound electron, with a screened residual contribution from the electron-attractive core. For an isoelectronic center with a hole-attractive local potential, on the other hand, the sequence of trapping an electron and a hole in forming a BX is reversed, i.e. the hole becomes the primary bound particle, and the electron is the secondary particle of the BX. When the screened residual contribution from the defect core potential is small, the secondary bound particle of the BX should be effective-masslike in terms of, for example, binding energy and g-factors. This can thus serve as a guideline in understanding the electronic structure of BXs. In our case of the I^* BX line, the deduced electron g-value is nearly identical to that of the conduction band electrons. However, the hole g-values are significantly different from the values of $g_h^{\parallel} = -(1.00 \div 1.3)$, $g_h^{\perp} = 0.1 \div 0.3$ deduced previously from D^0X^A that are relevant to the A-VB hole.[8,12,13,15] This finding provides strong evidence that the hole is the first and more tightly bound particle at the concerned isoelectronic center, which subsequently attracts a loosely bound electron that is effective-mass like. In other words, the center has a hole-attractive local potential.

VI. CONCLUSIONS

In conclusion, comprehensive time-resolved PL and magneto-optical measurements have been performed on the I^* transition, which has distinctly different magneto-optical properties as compared with that reported previously for

BX transitions in ZnO. From time-resolved PL spectroscopy, I^* is concluded to originate from the exciton ground state. From the temperature-dependent magneto-transmission and PL measurements, we showed that the I^* transition in fact arises from a BX bound to an isoelectronic center. Its electron and effective hole g-factors are derived as $g_e = 1.97$ and $g_h^{\parallel}(g_h^{\perp}) = 1.28(1.65)$, respectively. From a comparison of these values with that of the CB electron and VB hole, we were able to conclude that the involved isoelectronic center has a hole-attractive local potential such that the hole is the primary bound particle of the BX.

ACKNOWLEDGMENTS

Financial support by the Swedish Research Council (Grant No. 621-2010-3971) is greatly appreciated.

*Corresponding author: iribu@ifm.liu.se

[1]For a recent review, see, for example, C. Klingshirn, Phys. Status Solidi B **244**, 3027 (2007).
[2]B. K. Meyer, H. Alves, D. M. Hofmann, W. Kriegseis, D. Forster, F. Bertram, J. Christen, A. Hoffmann, M. Straßburg, M. Dworzak, U. Haboeck, and A. V. Rodina, Phys. Status Solidi B **241**, 231 (2004).
[3]For a recent review, see, for example, M. D. McCluskey and S. J. Jokela, J. Appl. Phys. **106**, 071101 (2009).
[4]Y. S. Park, C. W. Litton, T. C. Collins, and D. C. Reynolds, Phys. Rev. **143**, 512 (1966).
[5]G. Blattner, C. Klingshirn, R. Helbig, and R. Meinl, Phys. Status Solidi B **107**, 105 (1981).
[6]J. Gutowski, N. Presser, and I. Broser, Phys. Rev. B **38**, 9746 (1988).
[7]P. Loose, M. Rosenzweig, and M. Wöhlecke, Phys. Status Solidi B **75**, 137 (1976).
[8]A. V. Rodina, M. Strassburg, M. Dworzak, U. Haboeck, A. Hoffmann, A. Zeuner, H. R. Alves, D. M. Hofmann, and B. K. Meyer, Phys. Rev. B **69**, 125206 (2004).
[9]D. G. Thomas and J. J. Hopfield, Phys. Rev. **128**, 2135 (1962).
[10]D. C. Reynolds, D. C. Look, B. Jogai, C. W. Litton, G. Cantwell, and W. C. Harsch, Phys. Rev. B **60**, 2340 (1999).
[11]W. R. L. Lambrecht, A. V. Rodina, S. Limpijumnong, B. Segall, and B. K. Meyer, Phys. Rev. B **65**, 075207 (2002).
[12]M. R. Wagner, J.-H. Schulze, R. Kirste, M. Cobet, A. Hoffmann, C. Rauch, A. V. Rodina, B. K. Meyer, U. Röder, and K. Thonke, Phys. Rev. B **80**, 205203 (2009).
[13]L. Ding, B. K. Li, H. T. He, W. K. Ge, J. N. Wang, J. Q. Ning, X. M. Dai, C. C. Ling, and S. J. Xu, J. Appl. Phys. **105**, 053511 (2009).
[14]B. K. Meyer, J. Sann, S. Eisermann, S. Lautenschlaeger, M. R. Wagner, M. Kaiser, G. Callsen, J. S. Reparaz, and A. Hoffmann, Phys. Rev. B **82**, 115207 (2010).
[15]S. L. Chen, W. M. Chen, and I. A. Buyanova, Appl. Phys. Lett. **99**, 091909 (2011).
[16]H. Yoshida, H. Saito, and S. Shionoya, J. Phys. Soc. Jpn. **50**, 881 (1981).
[17]M. R. Wagner, G. Callsen, J. S. Reparaz, J.-H. Schulze, R. Kirste, M. Cobet, I. A. Ostapenko, S. Rodt, C. Nenstiel, M. Kaiser, A. Hoffmann, A. V. Rodina, M. R. Phillips, S. Lautenschläger, S. Eisermann, and B. K. Meyer, Phys. Rev. B **84**, 035313 (2011).
[18]E. I. Rashba and G. E. Gurgenishvili, Sov. Phys. Solid State **4**, 759(1962).
[19]G. Blattner, G. Kurtze, G. Schmieder, and C. Klingshirn, Phys. Rev. B **25**, 7413 (1982).
[20]D. G. Thomas, J. Phys. Chem. Solids **15**, 86 (1960).
[21]W. R. L. Lambrecht, A. V. Rodina, S. Limpijumnong, B. Segall, and B. K. Meyer, Phys. Rev. B **65**, 075207 (2002).
[22]D. C. Reynolds, C. W. Litton, and T. C. Collins, Phys. Rev. **140**, A1726 (1965).
[23]T. Sketrup, M. Suffczynski, and W. Gorzkowski, Phys. Rev. B **4**, 512 (1971).
[24]B. Monemar, U. Lindefelt, and W. M. Chen, Physica B **146**, 256 (1987).
[25]W. M. Chen, B. Monemar, and M. Godlewski, Diffus. Defect Data **62-63**, 133 (1989).